PERGAMON International Journal of Engineering Science 37 (1999) 1943–1957

International Journal of Engineering Science

www.elsevier.com/locate/ijengsci

Unsteady axisymmetric stagnation-point flow of a viscous fluid on a cylinder

H.S. Takhar [a,*], A.J. Chamkha [b], G. Nath [c]

[a] *School of Engineering, University of Manchester, Oxford Road, Manchester, M13 9PL, UK*
[b] *Department of Mechanical Engineering, Kuwait University, Kuwait*
[c] *Department of Mathematics, Indian Institute of Science, Bangalore, India*

Received 16 July 1998; received in revised form 7 October 1998; accepted 6 November 1998

(Communicated by E.S. ŞUHUBİ)

Abstract

The unsteady viscous flow in the vicinity of an axisymmetric stagnation point of an infinite circular cylinder is investigated when both the free stream velocity and the velocity of the cylinder vary arbitrarily with time. The cylinder moves either in the same direction as that of the free stream or in the opposite direction. The flow is initially ($t = 0$) steady and then at $t > 0$ it becomes unsteady. The semi-similar solution of the unsteady Navier–Stokes equations has been obtained numerically using an implicit finite-difference scheme. Also the self-similar solution of the Navier–Stokes equations is obtained when the velocity of the cylinder and the free stream velocity vary inversely as a linear function of time. For small Reynolds number, a closed form solution is obtained. When the Reynolds number tends to infinity, the Navier–Stokes equations reduce to those of the two-dimensional stagnation-point flow. The shear stresses corresponding to stationary and the moving cylinder increase with the Reynolds number. The shear stresses increase with time for the accelerating flow but decrease with increasing time for the decelerating flow. For the decelerating case flow reversal occurs in the velocity profiles after a certain instant of time.

1. Introduction

Most problems in fluid mechanics are similarity solutions in the sense that the number of independent variables is reduced by one or more. These similarity solutions may be derived by using

* Corresponding author. Tel.: 0044 161 275 4356; fax: 0044 161 275 4361.
E-mail address: hstakhar@fsl.eng.man.ac.uk (H.S. Takhar)

0020-7225/99/$ – see front matter
PII: S0020-7225(99)00009-9

(i) the dimensional arguments, (ii) the group-theoretic method (iii) or the ad hoc method of free parameters [1–5]. Hiemenz [6] has obtained an exact solution of the Navier–Stokes equations governing the two-dimensional stagnation-point flow on a flat plate. The analogous axisymmetric stagnation-point flow was investigated by Homann [7]. The solution of the Navier–Stokes equations governing the steady axisymmetric stagnation-point flow on an infinite stationary circular cylinder was obtained by Wang [8]. In a series of papers, Gorla [9–12] studied the steady and unsteady flows over a moving or stationary circular cylinder in the vicinity of the stagnation point under the boundary layer approximations.

In the present analysis, we have investigated the unsteady viscous flow in the vicinity of an axisymmetric stagnation point of an infinite circular cylinder when both the cylinder and the free stream velocities vary arbitrarily with time. A semi-similar solution of the unsteady Navier–Stokes equations has been obtained. It is also shown that when the cylinder and the free stream velocities vary inversely as a linear function of time, a self-similar solution exists. The non-linear partial differential equations governing the semi-similar flow and the non-linear ordinary differential equations governing the self-similar flow are solved numerically using an implicit finite-difference scheme and a shooting method, respectively. The results of the particular cases are compared with those of Wang [8], Gorla [10], Glauert [13] and Rott [14].

2. Problem formulation

We consider the laminar unsteady incompressible flow of a viscous fluid in the neighbourhood of an axisymmetric stagnation-point of an infinite circular cylinder when the free stream velocity and the cylinder velocity vary arbitrarily with time. The cylinder moves either in the same direction as that of the free stream velocity or in the direction opposite to it. Initially, (i.e., at $t=0$) the flow is steady and it becomes unsteady for $t>0$. A model of the flow and the co-ordinate system are shown in Fig. 1. The cylinder is described by $r=\mathrm{a}$ in the cylindrical polar co-ordinates. The flow is axisymmetric about the z-axis and also symmetric with respect to the $z=0$ plane. The stagnation line is at $z=0$, $r=\mathrm{a}$. The unsteady Navier-Stokes equations in cylindrical polar co-ordinates governing the axisymmetric flow are given by [8,10,12]

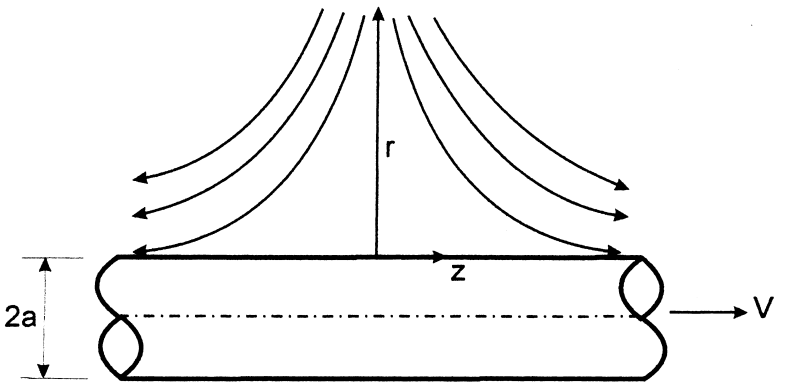

Fig. 1. Coordinate system and flow model.

$$\frac{\partial}{\partial r}(ru) + r\frac{\partial w}{\partial z} = 0, \tag{1}$$

$$\frac{\partial u}{\partial t} + u\frac{\partial u}{\partial r} + w\frac{\partial u}{\partial z} = -\frac{1}{\rho}\frac{\partial p}{\partial r} + v\left[\frac{\partial^2 u}{\partial r^2} + \frac{1}{r}\frac{\partial u}{\partial r} - \frac{u}{r^2} + \frac{\partial^2 u}{\partial z^2}\right], \tag{2}$$

$$\frac{\partial w}{\partial t} + u\frac{\partial w}{\partial r} + w\frac{\partial w}{\partial z} = -\frac{1}{\rho}\frac{\partial p}{\partial z} + v\left[\frac{\partial^2 w}{\partial r^2} + \frac{1}{r}\frac{\partial w}{\partial r} + \frac{\partial^2 w}{\partial z^2}\right]. \tag{3}$$

Far away from the cylinder the flow is inviscid and the potential velocity and the pressure distribution in the neighbourhood of the stagnation line are given by

$$\begin{aligned} U &= U_0\phi(t^*), \quad W = W_0\phi(t^*), \quad t^* = 2At, \quad U_0 = -A(r - a^2/r), \\ p_0 - p &= (\rho A^2/2)[(4z^2 + (r - a^2/r))\phi^2 + 2\{(2z^2 - r^2 + a^2 + 2a^2\log(r/a))\,\mathrm{d}\phi/\mathrm{d}t^*\}], \\ W_0 &= 2Az. \end{aligned} \tag{4}$$

We expect the viscous flow solution to approach the potential flow solution as $r \to \infty$. Here r and z are the radial and axial coordinates in the cylindrical polar co-ordinate system; u and w are the radial and axial velocities, respectively; ρ and p are the fluid density and the static pressure, respectively; v is the kinematic viscosity; U and W are the potential flow velocities in the radial and axial directions, respectively; U_0 and W_0 are the values of U and W at $t^* = 0$, respectively; t and t^* are the dimensional and the dimensionless times, respectively; A is a constant having the dimensions of t^{-1}; p_0 is the stagnation pressure; a is the radius of the circular cylinder and ϕ (t^*) is an arbitrary function of time t^*, having first order continuous derivative.

3. Semi-similar equations

It is possible to reduce the number of independent variables from three to two (i.e., semi-similar equations) by applying the following transformations:

$$\begin{aligned} \eta &= (r/a)^2, \quad t^* = 2At, \quad u = -A(a^2/r)\phi(t^*)f(\eta, t^*), \\ w &= [W_0 f'(\eta, t^*) + V_0 g'(\eta, t^*)]\phi(t^*), \quad \mathrm{Re} = 2^{-1}(Aa^2/v), \\ V &= V_0\phi(t^*), \quad w/V = [(W_0/V_0)f'(\eta, t^*) + g'(\eta, t^*)], \\ p_0 - p &= (\rho A^2/2)[4z^2(\phi^2 + \mathrm{d}\phi/\mathrm{d}t^* + p(\eta, t^*)] \end{aligned} \tag{5}$$

to Eqs. (1)–(3) and we find that Eq. (1) is identically satisfied and Eq. (3) reduces to

$$\eta f''' + f'' + \mathrm{Re}[\phi(1 + ff'' - f'^2) - (\partial f'/\partial t^*) + \phi^{-1}(\mathrm{d}\phi/\mathrm{d}t^*)(1 - f')] = 0, \tag{6}$$

$$\eta g''' + g'' + \mathrm{Re}[\phi(fg'' - f'g') - (\partial g'/\partial t^*) - \phi^{-1}(\mathrm{d}\phi/\mathrm{d}t^*)g'] = 0. \tag{7}$$

From Eq. (2), we get the expression for static pressures p (after integration)

$$p_0 - p = (\rho A^2/2)\left[4z^2(\phi^2 + \mathrm{d}\phi/\mathrm{d}t^*) - 2a^2\frac{\partial}{\partial t^*}\int_1^\eta (\phi f)\eta^{-1}\,\mathrm{d}\eta + (a\phi)^2(f^2/\eta) + 4(v\phi/A)f'\right]. \tag{8}$$

It may be noted that the expression for pressure p in Eq. (8) does not contain the function g', because g' occurs only in w and the term $w\,\partial u/\partial z$ in the equation for the radial pressure gradient $\rho^{-1}\partial p/\partial r$ vanishes as u is independent of z (see Eqs. (2) and (5)). However the expression for the axial pressure gradient $\rho^{-1}\partial p/\partial z$ in Eq. (3) does not contain g' and its derivatives which vanish by virtue of Eq. (7).

Eq. (6) is a third-order partial differential equation in f, but Eq. (7) is a second-order in g' (g does not occur in Eq. (7). Hence we can take $g' = h$). Therefore, three conditions are required for Eq. (6) and only two conditions are needed for Eq. (7). Since on the surface $\eta = 1$, no slip conditions have to be satisfied, $u = 0$, $w = V = V_0\ \phi\ (t^*)$ at $\eta = 1$ and as $\eta \to \infty$, $w \to W = W_0\phi(t^*) = 2Az\ \phi(t^*)$. Hence equating the coefficients of $2Az\phi(t^*)$ and $V_0\phi(t^*)$ on both sides in the expression for w in Eq. (5), we get the boundary conditions for Eqs. (6) and (7), as given by;

$$\begin{aligned} &f(1,t^*) = f'(1,t^*) = 0, \quad g'(1,t^*) = 1, \\ &f'(\infty,t^*) = 1, \quad g'(\infty,t^*) = 0. \end{aligned} \tag{9}$$

The initial conditions (i.e., conditions at $t^* = 0$) are given by the steady equations which are obtained from Eqs. (6) and (7) by putting $t^* = 0$, $\phi = 1$, $\mathrm{d}\phi/\mathrm{d}t^* = \partial f'/\partial t^* = \partial g'/\partial t^* = 0$ and these equations are given by

$$\eta f''' + f'' + \mathrm{Re}(1 + ff'' - f'^2) = 0, \tag{10}$$

$$\eta g''' + g'' + \mathrm{Re}(fg'' - f'g') = 0. \tag{11}$$

with boundary conditions

$$\begin{aligned} &f(1) = f'(1) = 0, \quad g'(1) = 1, \\ &f'(\infty) = 1, \quad g'(\infty) = 0. \end{aligned} \tag{12}$$

For the steady case ($t^* = 0$) the expression for pressure in Eq. (8) reduces to

$$p_0 - p = (\rho A^2/2)[4z^2 + a^2(f^2/\eta) + 4(v/A)f']. \tag{13}$$

It may be remarked that Eqs. (10)–(13) are identical to those of Wang [8] and Gorla [10]. From Eq. (8), the pressure p can be obtained after f and f' are determined from Eq. (6).

Here η is the dimensionless radial coordinate; f is the dimensionless radial velocity; f' is the dimensionless axial velocity for the stationary cylinder; g and g' are respectively, the dimensionless

radial and axial velocities corresponding to the moving cylinder; Re is the Reynolds number, and the prime denotes derivative with respect to η.

It is possible to obtain an asymptotic solution of Eqs. (6) and (7) for large Reynolds number Re. For small Re, the boundary layer is thick and for large Re it is thin. Hence for large Re, it is convenient to stretch both the independent and dependent variables by using the transformations,

$$\eta - 1 = (\mathrm{Re})^{-1/2}\xi, \quad f(\eta) = (\mathrm{Re})^{-1/2}F(\xi), \quad g(\eta) = (\mathrm{Re})^{-1/2}G(\xi). \tag{14}$$

Using the above transformations, Eqs. (6) and (7) can be expressed as

$$\left[1 + \xi(\mathrm{Re})^{-1/2}\right]\frac{\partial^3 F}{\partial \xi^3} + (\mathrm{Re})^{-1/2}\frac{\partial^2 F}{\partial \xi^2} + \left[\phi\left(1 + F\frac{\partial^2 F}{\partial \xi^2} - \left(\frac{\partial F}{\partial \xi}\right)^2\right) + \phi^{-1}\frac{\mathrm{d}\phi}{\mathrm{d}t^*}\left(1 - \frac{\partial F}{\partial \xi}\right) - \frac{\partial^2 F}{\partial t^* \partial \xi}\right] = 0, \tag{15}$$

$$\left[1 + \xi(\mathrm{Re})^{-1/2}\right]\frac{\partial^3 G}{\partial \xi^3} + (\mathrm{Re})^{-1/2}\frac{\partial^2 G}{\partial \xi^2} + \left[\phi\left(F\frac{\partial^2 G}{\partial \xi^2} - \frac{\partial F}{\partial \xi}\frac{\partial G}{\partial \xi}\right) - \phi^{-1}\frac{\mathrm{d}\phi}{\mathrm{d}t^*}\frac{\partial G}{\partial \xi} - \frac{\partial^2 G}{\partial t^* \partial \xi}\right] = 0, \tag{16}$$

Boundary conditions (9) can be rewritten as

$$F(0,t^*) = \frac{\partial F}{\partial \xi}(0,t^*) = 0, \quad G(0,t^*) = 0, \quad \frac{\partial G}{\partial \xi}(0,t^*) = 1,$$
$$\frac{\partial F}{\partial \xi}(\infty,t^*) = 1, \quad \frac{\partial G}{\partial \xi}(\infty,t^*) = 0. \tag{17}$$

When $\mathrm{Re} \to \infty$, Eqs. (15) and (16) reduce to

$$\frac{\partial^3 F}{\partial \xi^3} + \left[\phi\left(1 + \frac{\partial F}{\partial \xi}\frac{\partial^2 F}{\partial \xi^2} - \left(\frac{\partial F}{\partial \xi}\right)^2\right) + \phi^{-1}\frac{\mathrm{d}\phi}{\mathrm{d}t^*}\left(1 - \frac{\partial F}{\partial \xi}\right) - \frac{\partial^2 F}{\partial t^* \partial \xi}\right] = 0, \tag{18}$$

$$\frac{\partial^3 G}{\partial \xi^3} + \left[\phi\left(F\frac{\partial^2 G}{\partial \xi^2} - \frac{\partial F}{\partial \xi}\frac{\partial G}{\partial \xi}\right) - \phi^{-1}\frac{\mathrm{d}\phi}{\mathrm{d}t^*}\frac{\partial G}{\partial \xi} - \frac{\partial^2 G}{\partial t^* \partial \xi}\right] = 0. \tag{19}$$

It may be remarked that Eq. (18) represents the unsteady two-dimensional stagnation-point flow for an arbitrary time-dependent variation of the free stream velocity. Also, for $t^* = \mathrm{d}\phi/\mathrm{d}t^* = \partial^2 F/\partial t^* \partial \xi = 0$, $\phi = 1$, Eq. (18) reduces to the well known Hiemenz flow [6]. Also, Eq. (19) represents the unsteady flow over a moving wall and the corresponding steady case has been studied by Glauert [13] and Rott [14].

If the Reynolds number Re is very small ($\mathrm{Re} \to 0$), Eqs. (6) and (7) under conditions (9) yield, as a first approximation, a closed form solution

$$f = b(t^*)[\eta \log\eta - \eta + 1], \tag{20a}$$

$$g' = c(t^*) \log\eta + 1, \tag{20b}$$

which is singular at infinity. The above solutions breakdown for $\eta = 0(1/\mathrm{Re})$. For the steady case, b and c are constants and Eq. (20a) is the same as that of Wang [8], who considered the steady stagnation-point flow on a stationary cylinder.

The skin friction coefficient in the axial direction is expressed as

$$C_f = \mu(\partial w/\partial r)_{r=a}/(\rho V_0^2) = 2(\mathrm{Re_a})^{-1}[(W_0/V_0)f''(1,t^*) + g''(1,t^*)]\phi(t^*), \tag{20c}$$

where $\mathrm{Re_a} = V_0 a/v$ is the Reynolds number.

4. Self-similar equations

It may be remarked that Eqs. (1)–(3) can be reduced to a system of ordinary differential equations if we assume that the free stream velocity components in the r- and z-directions, U and W, and the velocity of the cylinder V all vary inversely as a linear function of time t^* (i.e., $U = U_0(1-\lambda t^*)^{-1}$, $W = W_0(1-\lambda t^*)^{-1}$, $V = V_0(1-\lambda t^*)^{-1}$ where U_0, W_0 and V_0 are, respectively, the radial, axial and wall velocities at $t^* = 0$). We apply the following transformations

$$\eta = (r/a)^2(1-\lambda t^*)^{-1/2}, \quad \lambda t^* < 1, \quad t^* = 2At, \quad U_0 = -A(r - a^2/r),$$

$$W_0 = 2Az, \quad u = -(Aa^2/r)(1-\lambda t^*)^{-1/2} f(\eta),$$

$$w = 2Az(1-\lambda t^*)^{-1} f'(\eta) + V_0(1-\lambda t^*)^{-1} g'(\eta), \quad \overline{\mathrm{Re}} = \mathrm{Re}(1-\lambda t^*)^{-1/2},$$

$$p_0 - p = 2\rho A a^2 (1-\lambda t^*)^{-2}[(1+\lambda)z^2 + 2(1-\lambda/2)(1-\lambda t^*)(v/A)P(\eta)], \tag{21}$$

to Eqs. (1)–(3) and we find that Eq. (1) is satisfied identically and Eq. (3) yields

$$\eta f''' + f'' + \overline{\mathrm{Re}}[1 + ff'' - (f')^2 + \lambda(1 - f' - \eta f''/2)] = 0, \tag{22}$$

$$\eta g''' + g'' + \overline{\mathrm{Re}}[(fg'' - f'g') - \lambda(g' + \eta g''/2)] = 0. \tag{23}$$

The boundary conditions are given by

$$\begin{aligned} &\text{at } \eta = (1-\lambda)^{-1/2}: f = f' = 0, \quad g' = 1, \\ &\text{at } \eta \to \infty: f' \to 1, \quad g' \to 0. \end{aligned} \tag{24}$$

From Eqs. (2) and (21), we get the expression for the dimensionless pressure $P(\eta)$ in the form

$$(1-\lambda/2)P = 2^{-1} f' + 4^{-1}\left(\overline{\mathrm{Re}}\right)\left(f^2/\eta\right) - 4^{-1}\lambda\overline{\mathrm{Re}}\left[\int_{(1-\lambda t^*)^{-1/2}}^{\eta} (f/\eta)\, \mathrm{d}\eta + f\right]. \tag{25}$$

Since the boundary condition $\eta = (1-\lambda t^*)^{-1/2}$ is a function of time t^*, in order to make it constant, we change both the independent and dependent variables, which are given by

$$\xi = \eta(1-\lambda t^*)^{1/2}, \quad f(\eta) = (1-\lambda t^*)^{-1/2}\, F(\xi), \quad g(\eta) = (1-\lambda t^*)^{-1/2}\, G(\xi). \tag{26}$$

Using the above transformations, Eqs. (22) and (23) reduce to

$$\xi\frac{\mathrm{d}^3F}{\mathrm{d}\xi^3} + \frac{\mathrm{d}^2F}{\mathrm{d}\xi^2} + \overline{\mathrm{Re}}\left[1 + F\frac{\mathrm{d}^2F}{\mathrm{d}\xi^2} - \left(\frac{\mathrm{d}F}{\mathrm{d}\xi}\right)^2 + \lambda\left(1 - \frac{\mathrm{d}F}{\mathrm{d}\xi} - 2^{-1}\xi\frac{\mathrm{d}^2F}{\mathrm{d}\xi^2}\right)\right] = 0, \tag{27}$$

$$\xi\frac{\mathrm{d}^3G}{\mathrm{d}\xi^3} + \frac{\mathrm{d}^2G}{\mathrm{d}\xi^2} + \overline{\mathrm{Re}}\left[\left(F\frac{\mathrm{d}^2G}{\mathrm{d}\xi^2} - \frac{\mathrm{d}F}{\mathrm{d}\xi}\frac{\mathrm{d}G}{\mathrm{d}\xi}\right) - \lambda\left(\frac{\partial G}{\mathrm{d}\xi} + 2^{-1}\xi\frac{\mathrm{d}^2G}{\mathrm{d}\xi^2}\right)\right] = 0. \tag{28}$$

Boundary conditions (24) can be rewritten as

$$\begin{aligned} &\xi = 1: F = \mathrm{d}F/\mathrm{d}\xi = 0, \quad G = 0, \quad \mathrm{d}G/\mathrm{d}\xi = 1, \\ &\xi \to \infty: \mathrm{d}F/\mathrm{d}\xi \to 1; \quad \mathrm{d}G/\mathrm{d}\xi \to 0. \end{aligned} \tag{29}$$

The expression for pressure p is given by

$$\begin{aligned} p_0 - p = 2\rho A^2(1-\lambda t^*)^{-2}\Bigg[&(1+\lambda)z^2 + (2v/A)\{2^{-1}(1-\lambda t^*)(\mathrm{d}F/\mathrm{d}\xi) + 4^{-1}\overline{\mathrm{Re}}(F^2/\xi) \\ &- 4^{-1}\overline{\mathrm{Re}}\lambda\left(\int_1^{\xi}(F/\xi)\,\mathrm{d}\xi + F\right)\Bigg]. \end{aligned} \tag{30}$$

For the steady-state case $\lambda = 0$, $\overline{\mathrm{Re}} = \mathrm{Re}$. Using the transformations similar to Eq. (14), viz

$$\xi - 1 = \left(\overline{\mathrm{Re}}\right)^{-1/2}X, \quad F(\xi) = \left(\overline{\mathrm{Re}}\right)^{-1/2}H(X), \quad G(\xi) = \left(\overline{\mathrm{Re}}\right)^{-1/2}S(X), \tag{31}$$

Eqs. (27) and (28) with $\lambda = 0$ tend, respectively to the Hiemenz flow [6] and the flow over a moving plate [13,14] when $\overline{\mathrm{Re}} = \mathrm{Re} \to \infty$. The resulting steady-state equations are given by

$$\frac{\mathrm{d}^3H}{\mathrm{d}X^3} + H\frac{\mathrm{d}^2H}{\mathrm{d}X^2} + 1 - \left(\frac{\mathrm{d}H}{\mathrm{d}X}\right)^2 = 0, \tag{32}$$

$$\frac{\mathrm{d}^3S}{\mathrm{d}X^3} + H\frac{\mathrm{d}^2S}{\mathrm{d}X^2} - \frac{\mathrm{d}H}{\mathrm{d}X}\frac{\mathrm{d}S}{\mathrm{d}X} = 0, \tag{33}$$

with boundary conditions

$$\begin{aligned} &\text{at } X = 0 := H = \mathrm{d}H/\mathrm{d}X = 0, \quad S = 0, \quad \mathrm{d}S/\mathrm{d}X = 1, \\ &\text{as } X \to \infty := \mathrm{d}H/\mathrm{d}X \to 1, \quad \mathrm{d}S/\mathrm{d}X \to 0. \end{aligned} \tag{34}$$

The skin friction coefficient in the axial direction C_f for the self-similar case is given by;

$$C_f = \mu(\partial w/\partial r)_{r=a}/(\rho V^2) = 2(\mathrm{Re}_a)^{-1}(1-\lambda t^*)^{1/2}(W_0/V_0)f''(1) + g''(1)]. \tag{35}$$

5. Method of solution

The partial differential equations (6) and (7) under the initial and boundary conditions (9)–(12) are solved numerically by an implicit, iterative tri-diagonal finite-difference method similar to that discussed by Blottner [15]. All the first order derivative with respect to t^* are replaced by two-point backward difference formulae of the form

$$\partial B/\partial t^* = (B_{m,n} - B_{m-1,n})/\Delta t^*, \tag{36}$$

where B is any dependent variable and m and n are the node locations along t^* and η directions, respectively. First the third-order differential equations (6) and (7) are converted into second-order by substituting $H_1 = f'$ and $S_1 = g'$, respectively. Then the second-order differential equation for H_1 and S_1 are discretized using three-point central difference formulae while all first-order differential equations are discretized by employing the trapezoidal rule. At each line of constant t^*, a system of algebraic equations is obtained. With the non-linear terms evaluated at the previous iteration, the algebraic equations are solved iteratively by using the well known Thomas algorithm (see Ref. [15]). The same process is repeated for the next t^* value and the problem is solved line by line until the desired t^* value is reached. A convergence criterion based on the relative difference between the current and previous iterations is employed. When this difference reaches 10^{-5}, the solution is assumed to have converged and the iterative process is terminated.

Ordinary differential equations (26) and (27) under conditions (29) governing the self-similar flow are also solved numerically using a shooting method which is described in detail by Takhar [16].

We have examined the effect of the grid size $\Delta\eta$ and Δt^*, and the edge of the boundary layer η_∞. The results presented here are independent of the grid size and η_∞ up to the 4th decimal place.

6. Results and discussion

Eqs. (6) and (7) under conditions (9)–(12) and Eqs. (27) and (28) under boundary conditions (29) were solved numerically using the methods described earlier. To validate our results we have compared our steady-state results for the surface shear stresses $(\mathrm{Re}^{-1/2}f''(1), \mathrm{Re}^{-1/2}g''(1))$ with those of Wang [8] and Gorla [10]. We have also compared the surface shear stresses, $(H''(0), -S''(0))$, for the steady case when $\mathrm{Re} \to \infty$, where $H' = \mathrm{d}H/\mathrm{d}\xi, S' = \mathrm{d}S/\mathrm{d}\xi$) with those of Refs. [6,13,14]. In all the cases, the results are found to be in very good agreement (the maximum difference is less than 1 per cent). Since the results are tabulated by Wang [8] and Gorla [10], for the sake of brevity, the comparison is not given here.

The surface shear stresses corresponding to the stationary and the moving cylinder for the accelerating case $(\phi(t^*) = 1 + \epsilon t^{*2}, \epsilon > 0)$ and decelerating case $(\phi(t^*) = 1 - \epsilon t^{*2}, \epsilon > 0)$, and for several values of the Reynolds number Re are presented in Figs. 2–5. The shear stresses $(f''(1,t^*), -g''(1,t^*))$ are found to increase with the Reynolds number Re. An increase in the

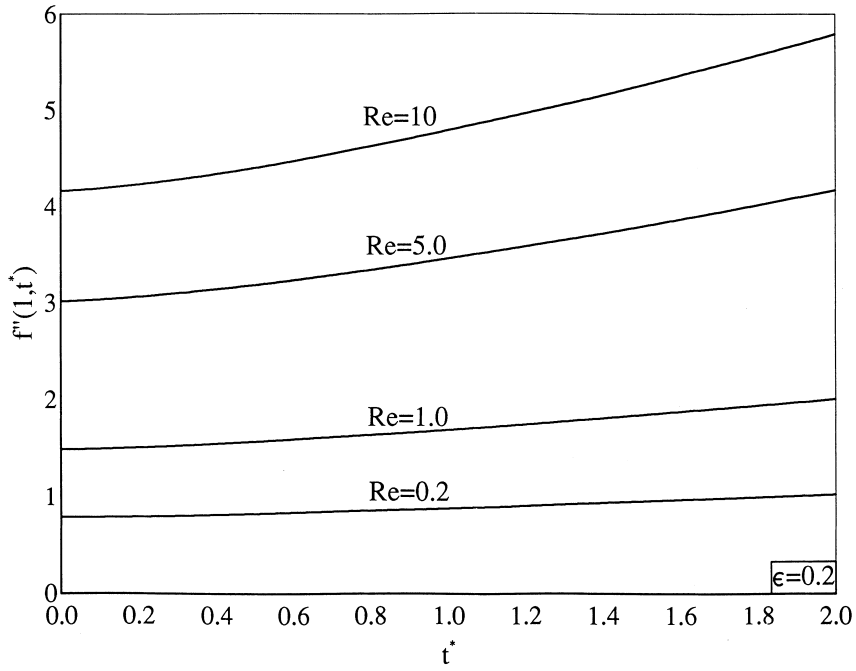

Fig. 2. Variation of the surface shear stress $f''(1,t^*)$ with time t^* for $\phi(t^*) = 1 + \epsilon t^{*2},\ \epsilon = 0.2,\ \mathrm{Re} = 0.2, 1.0, 5.0, 10.0$.

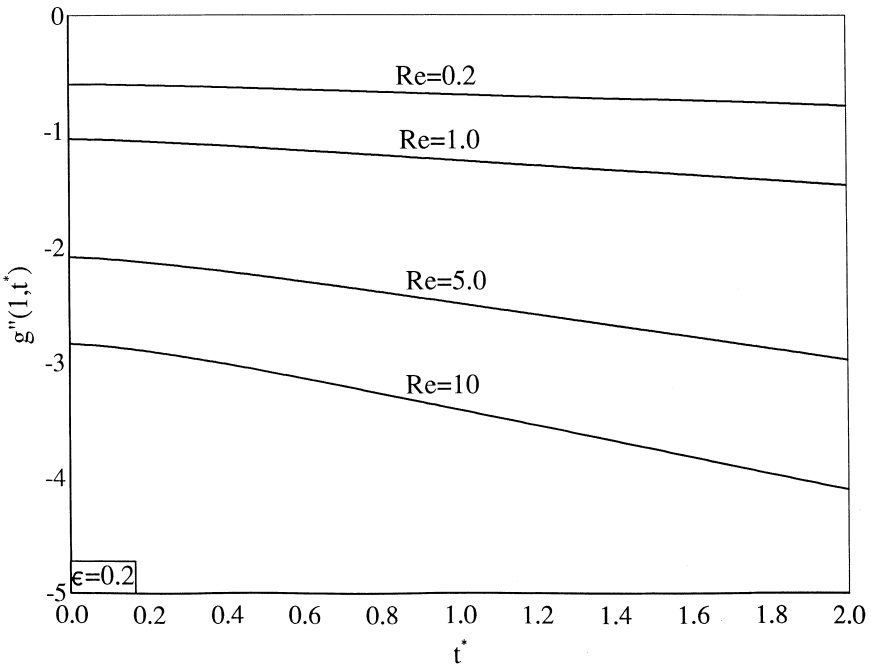

Fig. 3. Variation of the surface shear stress $g''(1,t^*)$ with time t^* for $\phi(t^*) = 1 + \epsilon t^{*2},\ \epsilon = 0.2,\ \mathrm{Re} = 0.2, 1.0, 5.0, 10.0$.

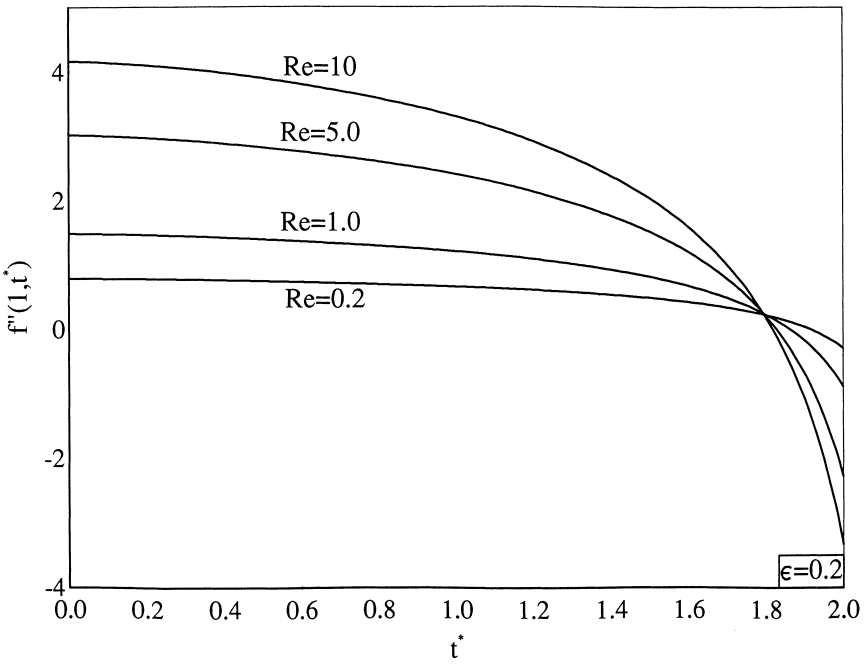

Fig. 4. Variation of the surface shear stress $f''(1,t^*)$ with time t^* for $\phi(t^*) = 1 - \epsilon t^{*2},\ \epsilon = 0.2,\ \mathrm{Re} = 0.2, 1.0, 5.0, 10.0$.

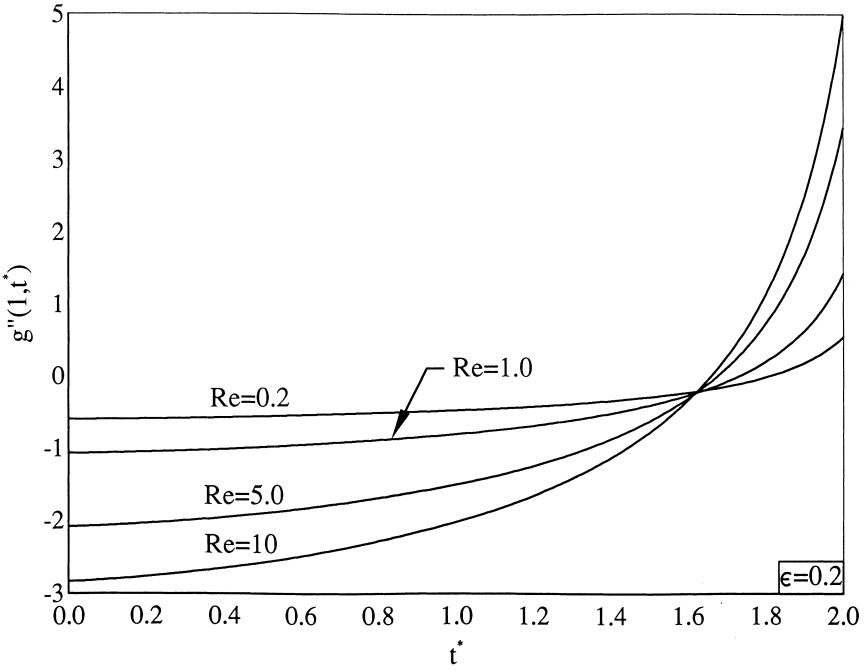

Fig. 5. Variation of the surface shear stress $g''(1,t^*)$ with time t^* for $\phi(t^*) = 1 - \epsilon t^{*2},\ \epsilon = 0.2,\ \mathrm{Re} = 0.2, 1.0, 5.0, 10.0$.

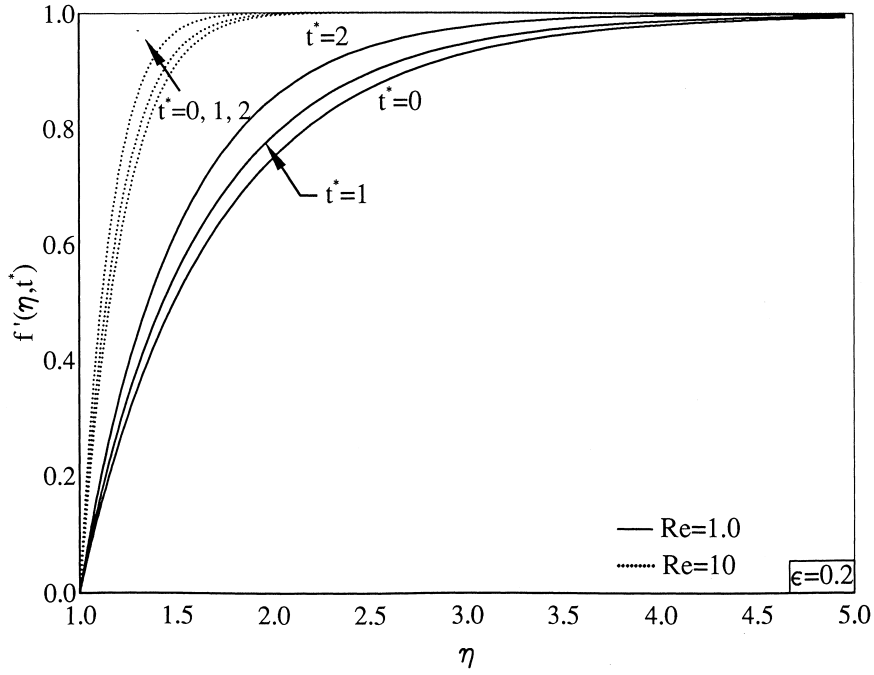

Fig. 6. Velocity profiles $f'(\eta, t^*)$ for $\phi(t^*) = 1 + \epsilon t^{*2}$, $\epsilon = 0.2$, $t^* = 0, 1, 2$, $\mathrm{Re} = 1.0, 10.0$.

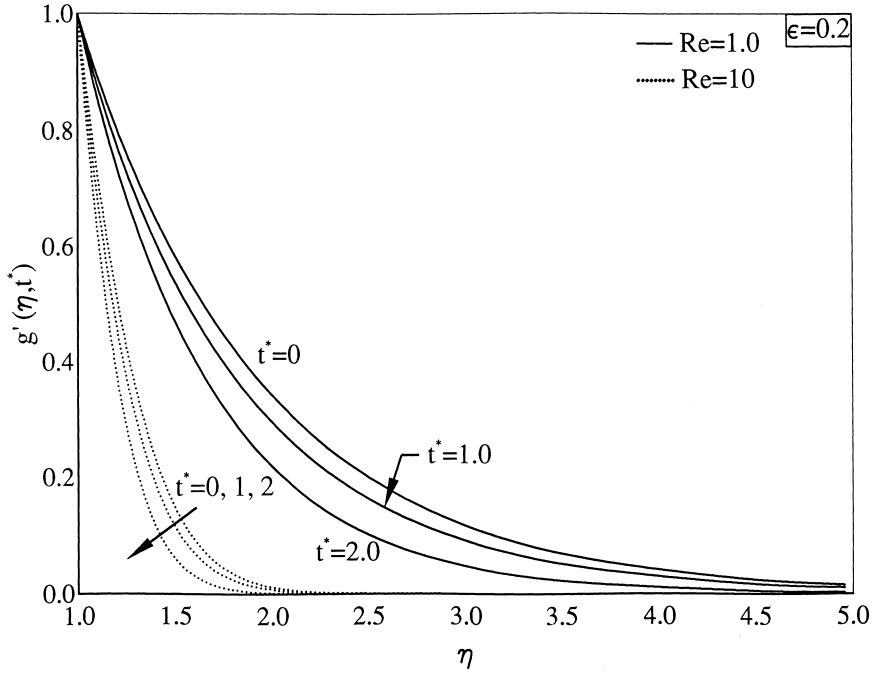

Fig. 7. Velocity profiles $g'(\eta, t^*)$ for $\phi(t^*) = 1 + \epsilon t^{*2}$, $\epsilon = 0.2$, $t^* = 0, 1, 2$, $\mathrm{Re} = 1.0, 10.0$.

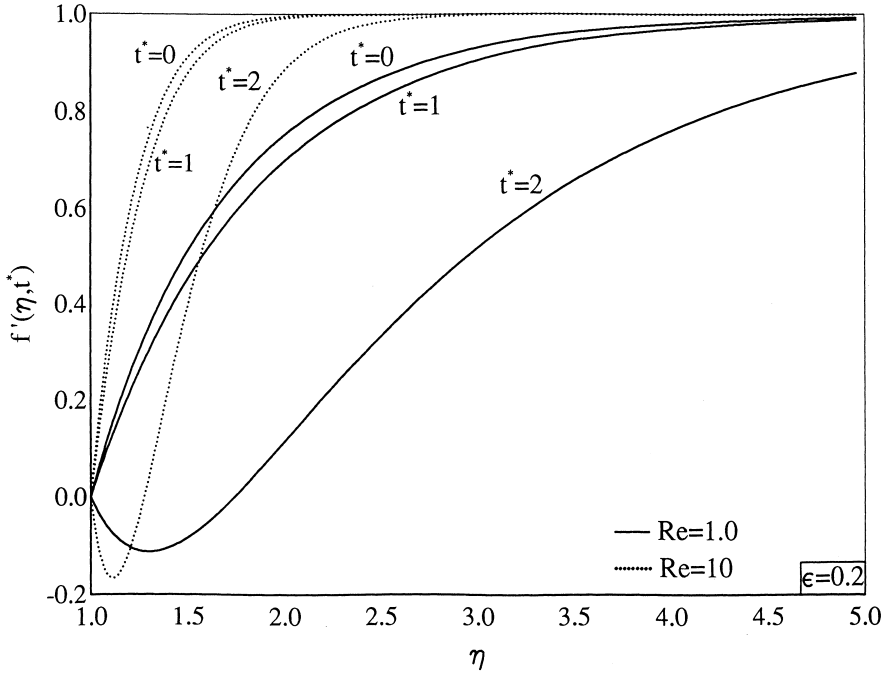

Fig. 8. Velocity profiles $f'(\eta, t^*)$ for $\phi(t^*) = 1 - \epsilon t^{*2}$, $\epsilon = 0.2$, $t^* = 0, 1, 2$, $\mathrm{Re} = 1.0, 10.0$.

Reynolds number implies either an increase in the free stream velocity or a reduction in the kinematic viscosity. Consequently, the boundary layer thickness is reduced and hence the shear stresses are increased. The shear stresses also increase with time t^* for the accelerating case $(\phi(t^*) = 1 + \epsilon t^{*2}, \epsilon > 0)$ and they decrease for decelerating case $(\phi(t^*) = 1 - \epsilon t^{*2}, \epsilon > 0)$. The reason for this behaviour is that the increase in the free stream velocity or surface velocity imparts additional momentum into the flow field causing an increase in the surface shear stresses with time t^*. The effect in the case of decelerating flow is just the opposite. An interesting result for the decelerating flow $(\phi(t^*) = 1 - \epsilon t^{*2}, \epsilon > 0)$ is that the shear stresses $f''(1, t^*) \gtrless 0$ for $t^* \lessgtr t_0^*$ and $-g''(1, t^*) \lessgtr 0$ for $t^* \lessgtr t_1^*$ (see Figs. 4 and 5). This implies that the reverse flow occurs in the velocity profile $f'(\eta, t^*)$ near the wall when $t^* > t_0^*$ and in $g'(\eta, t^*)$ when $t^* > t_1^*$ as is evident from Figs. 8 and 9. It may be remarked that the vanishing of shear stress at the wall does not imply separation for unsteady flows [17]. The reverse flow is due to the growth in the boundary layer thickness which is caused by the reduction in the free stream or the wall velocity with increasing time. We have also compared our shear stresses, $\mathrm{Re}^{-1/2} f''(1, t^*)$ and $\mathrm{Re}^{-1/2} g''(1, t^*)$ for $\mathrm{Re} = 100$, $t^* = 1$ with the two-dimensional stagnation-point results obtained from Eqs. (18) and (19). We find that the results agree within 2.5 per cent which implies that the cylindrical curvature effect becomes less important for high Reynolds number. Similar trend was observed by Gorla [10] for the steady case.

Figs. 6 and 7 show the velocity profiles $f'(\eta, t^*)$ and $g'(\eta, t^*)$ at different instants of time t^* for $\mathrm{Re} = 1$ and $10, \phi(t^*) = 1 + \epsilon t^{*2}$, $\epsilon = 0.2$ (accelerating flow). The velocity profiles $f'(\eta, t^*)$ and $g'(\eta, t^*)$ increase with increasing time t^* and Reynolds number Re, because for an accelerating flow the fluid in the viscous layer gets accelerated. The corresponding results for the decelerating flow $(\phi(t^*) = 1 - \epsilon t^{*2}, \epsilon = 0.2)$ are presented in Figs. 8 and 9. In this case, the velocity profiles $f'(\eta, t^*)$

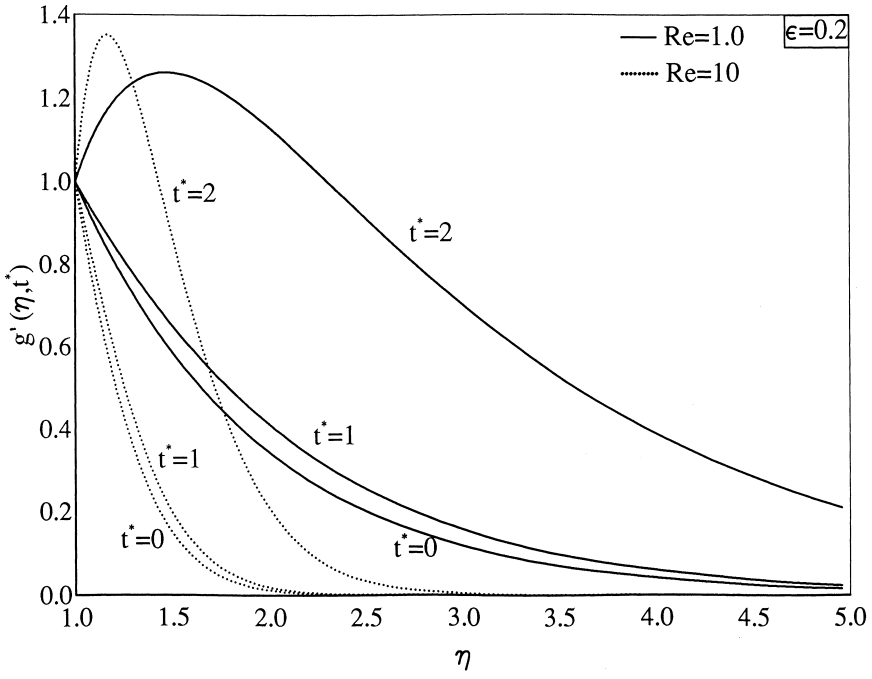

Fig. 9. Velocity profiles $g'(\eta, t^*)$ for $\phi(t^*) = 1 - \epsilon t^{*2}$, $\epsilon = 0.2$, $t^* = 0, 1, 2$, $\mathrm{Re} = 1.0, 10.0$.

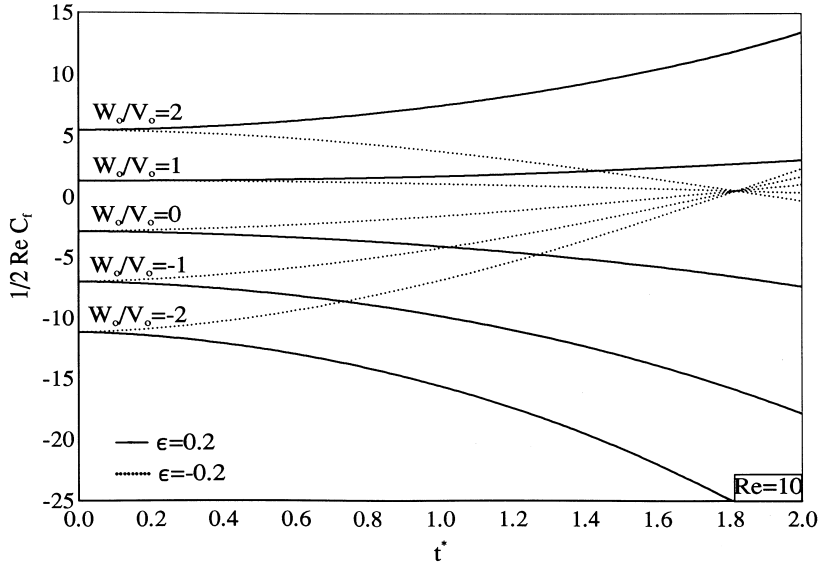

Fig. 10. Skin friction coefficient $(2^{-1}\,\mathrm{Re}_a\,C_f)$ time history for $\phi(t^*) = 1 + \epsilon t^{*2}$, $\epsilon = \pm 0.2$, $\mathrm{Re} = 10.0$, $W_0/V_0 = -2, -1, 0, 1, 2$.

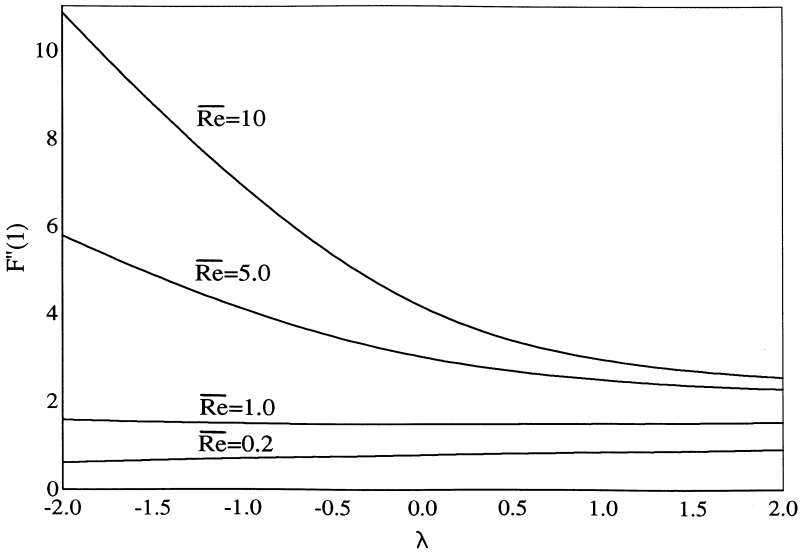

Fig. 11. Variation of the surface shear stress F'' (1) with λ and $\overline{\mathrm{Re}}$.

and $g'(\eta, t^*)$ decrease with increasing time t^*, but they increase with Reynolds number Re. Also for $t^* = 2$ reverse flow occurs in the velocity profiles $f'(\eta, t^*)$ and $g'(\eta, t^*)$ as mentioned earlier.

Fig. 10 shows the variation of the surface skin friction coefficient $2^{-1}\mathrm{Re}_a C_f$ with time t^* for $\mathrm{Re} = 10$, $\phi(t^*) = 1 + \epsilon t^{*2}$, $\epsilon = \pm 0.2$ and $-2 \leqslant W_0/V_0 \leqslant 2$ (i.e., when the free stream and surface velocities are in the same directions $(W_0/V_0 > 0)$ or in the opposite directions $(W_0/V_0 < 0)$. The skin friction coefficient for $W/V_0 \leqslant 0$ increases with time t^* for accelerating flow

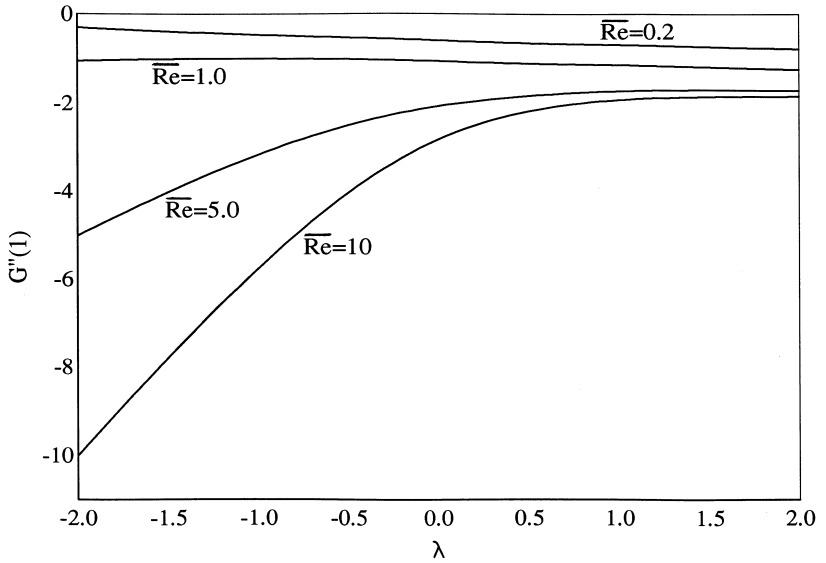

Fig. 12. Variation of the surface shear stress G'' (1) with λ and $\overline{\mathrm{Re}}$.

($\phi(t^*) = 1 + \epsilon t^{*2}, \epsilon = 0.2$), but decreases with time for decelerating flow ($\phi(t^*) = 1 - \epsilon t^{*2}, \epsilon = 0.2$). However, for $W_0/V_0 \geqslant 1$, the skin friction coefficient displays an opposite trend. Also it vanishes for certain values of W_0/V_0 , but it does not imply separation [17].

For self-similar flow (Eqs. (27)–(29)) the variation of the surface shear stresses $F''(1)$ and $G''(1)$ with the Reynolds number $\overline{\mathrm{Re}}$ and the unsteady parameter λ is presented in Figs. 11 and 12. Both $F''(1)$ and $G''(1)$ increase with $\overline{\mathrm{Re}}$, because the fluid gets accelerated with increasing $\overline{\mathrm{Re}}$ which results in a thinner boundary layer. The effect of λ is more pronounced for $\overline{\mathrm{Re}} > 1$.

7. Conclusions

The surface shear stresses increase with the Reynolds number and time for accelerating flow. For a decelerating flow, they increase with the Reynolds number upto a certain instant of time, but they decrease with increasing time for all Reynolds number. For decelerating flow the shear stresses vanish at a certain instant of time, and after that time reverse flow occurs in the velocity profiles. For $\mathrm{Re} \to \infty$ the solution of the Navier–Stokes equations tends to the solution of the two-dimensional stagnation-point flow.

References

[1] G. Birkoff, Hydrodynamics: A study of Logic, Fact and Similitude, Princeton University Press, Princeton, 1960.
[2] G.W. Blueman, J.D. Cole, Similarity Method for Differential Equations, Springer, New York, 1974.
[3] L.V. Ovsiannikov, Group Analysis of Differential Equations, Academic Press, New York, 1982.
[4] P.J. Olver, Applications of Lie Groups to Differential Equations, Springer, Berlin, 1986.
[5] P.K.H. Ma, W.H. Hui, Similarity solutions of the two-dimensional unsteady boundary layer equations, J. Fluid Mech. 216 (1990) 537–559.
[6] K. Hiemenz, Die Granzschicht an einem in den gleich formigen Flussigkeitsstrom eingetauchten geraden Kreszylinder, Dinglers Polytech. J. 326 (1911) 321–324.
[7] F. Homann, Der Einfluss grosser zähigkeit bei der Strömung um den zylinder und um die Kugel, ZAMM 16 (1936) 153–164.
[8] C.Y. Wang, Axisymmetric stagnation flow on a cylinder, Quart. Appl. Math. 43 (1974) 209–215.
[9] R.S.R. Gorla, Unsteady laminar axisymmetric stagnation flow over a circular cylinder, Dev. Mech. 9 (1977) 286–288.
[10] R.S.R. Gorla, Nonsimilar axisymmetric stagnation flow on a moving cylinder, Int. J. Engng. Sci. 16 (1978) 397–400.
[11] R.S.R. Gorla, Transient response behaviour of an axisymmetric stagnation flow on a circular cylinder due to time dependent free stream velocity, Int. J. Engng. Sci. 16 (1978) 493–502.
[12] R.S.R. Gorla, Unsteady viscous flow in the vicinity of an axisymmetric stagnation-point on a circular cylinder, Int. J. Engng. Sci. 17 (1979) 87–93.
[13] M.B. Glauert, The laminar boundary layer on oscillating plates and cylinders, J. Fluid Mech. 1 (1956) 97–110.
[14] N. Rott, Quart. Unsteady wedge flow in the vicinity of a stagnation point, Quart. Appl. Math. 13 (1956) 444–451.
[15] F.G. Blottner, Finite-difference methods of solution of the boundary layer equations, AIAA.J. 8 (1970) 193–205.
[16] H.S. Takhar, Free convection from a flat plate, J. Fluid Mech. 34 (1968) 81–89.
[17] W.R. Sears, D.P. Telionis, Boundary layer separation in unsteady flow, SIAM J. Appl. Math. 28 (1975) 215–235.